JVSTA Journal of Vacuum Science & Technology A

Use of B2O3 films grown by plasma-assisted atomic layer deposition for shallow boron doping in silicon

Bodo Kalkofen, Akinwumi A. Amusan, Muhammad S. K. Bukhari, Bernd Garke, Marco Lisker, Hassan Gargouri, and Edmund P. Burte

Citation: Journal of Vacuum Science & Technology A **33**, 031512 (2015); doi: 10.1116/1.4917552
View online: http://dx.doi.org/10.1116/1.4917552
View Table of Contents: http://scitation.aip.org/content/avs/journal/jvsta/33/3?ver=pdfcov
Published by the AVS: Science & Technology of Materials, Interfaces, and Processing

Use of B_2O_3 films grown by plasma-assisted atomic layer deposition for shallow boron doping in silicon

Bodo Kalkofen,[a] Akinwumi A. Amusan, and Muhammad S. K. Bukhari
Institute of Micro and Sensor Systems, Otto-von-Guericke University, Universitätsplatz 2, 39106 Magdeburg, Germany

Bernd Garke
Institute for Experimental Physics, Otto-von-Guericke University, Universitätsplatz 2, 39106 Magdeburg, Germany

Marco Lisker
IHP, Im Technologiepark 25, 15236 Frankfurt (Oder), Germany

Hassan Gargouri
SENTECH Instruments GmbH, Schwarzschildstraße 2, 12489 Berlin, Germany

Edmund P. Burte
Institute of Micro and Sensor Systems, Otto-von-Guericke University, Universitätsplatz 2, 39106 Magdeburg, Germany

(Received 7 January 2015; accepted 3 April 2015; published 15 April 2015)

Plasma-assisted atomic layer deposition (PALD) was carried for growing thin boron oxide films onto silicon aiming at the formation of dopant sources for shallow boron doping of silicon by rapid thermal annealing (RTA). A remote capacitively coupled plasma source powered by GaN microwave oscillators was used for generating oxygen plasma in the PALD process with tris(dimethylamido)borane as boron containing precursor. ALD type growth was obtained; growth per cycle was highest with 0.13 nm at room temperature and decreased with higher temperature. The as-deposited films were highly unstable in ambient air and could be protected by capping with *in-situ* PALD grown antimony oxide films. After 16 weeks of storage in air, degradation of the film stack was observed in an electron microscope. The instability of the boron oxide, caused by moisture uptake, suggests the application of this film for testing moisture barrier properties of capping materials particularly for those grown by ALD. Boron doping of silicon was demonstrated using the uncapped PALD B_2O_3 films for RTA processes without exposing them to air. The boron concentration in the silicon could be varied depending on the source layer thickness for very thin films, which favors the application of ALD for semiconductor doping processes. © *2015 American Vacuum Society*. [http://dx.doi.org/10.1116/1.4917552]

I. INTRODUCTION

Boron is an important dopant for semiconductor materials such as silicon and germanium. For increased performance and integration of semiconductor devices, their dimensions are continuously scaled down, and new device structures like FinFETs, nanowires, and other three-dimensional (3D) surface configurations become more and more important. The doping technology for such structures is challenging, and conventional doping methods need to be adapted or replaced. The well-established ion-implantation faces here severe limitations due to its radiative nature, which leads to structural damage, channeling in crystalline materials and shadowing effects at 3D surface features. Alternatives like plasma doping[1] were investigated in order to overcome limitations of conventional implantation, but problematic damage-related phenomena as transient enhanced diffusion during dopant activation and shadowing effects due to showers of directed species cannot be fully avoided. The more historical technique of solid-phase diffusion from pre-deposited glass layers or high-temperature gas-phase depositions lacks in most cases the needed uniformity and dose control. Several nonradiative alternatives were proposed and are under current investigation as doping from molecular monolayers,[2,3] from spin-on dopant (SOD) boron source,[4] or vapor phase doping using BBr_3 gas.[5] It is obvious that the method of controlled deposition of the dopant source is a key issue that needs to be addressed. In previous publications, the application of atomic layer deposition was suggested for that purpose,[6,7] applying the potential of precise control of deposition and material properties of this technique. The investigation of plasma-assisted ALD processes for the deposition of boron oxide and successive drive-in of boron into silicon will be presented here. Only some work on ALD of B_2O_3 has been reported so far. Putkonen and Niinistö[8] used boron bromide and water as precursor for deposition at room temperature. The ALD of B_2O_3 using tris(dimethylamido)borane and ozone was presented in earlier papers.[7,9] Growth could be observed from room temperature up to 100 °C, but growth per cycle decreased significantly with increasing temperature. The as-deposited films

[a]Electronic mail: bodo.kalkofen@ovgu.de

showed high volatility in ambient air, which could directly observed during *ex-situ* time-dependent ellipsometric film thickness measurements. The application of these films for shallow boron doping of silicon could be shown. Very recently, the ALD of B_2O_3/SiO_2 layers was investigated for dopant applications as well.[10] There, trimethylborate was used as boron precursor and H_2O, O_3, and O_2 plasma were investigated as oxidants at a deposition temperature of 150 °C. The ALD of SiO_2 was applied for stabilization of the volatile B_2O_3 films and it could be proved by XPS measurements that the boron oxide films showed B_2O_3 type stoichiometry. Other beneficial properties of B_2O_3 material, like its effectiveness as solid lubricant, were investigated as well[11] and different deposition techniques for thin films of this material such as MOCVD (Ref. 12) and magnetron sputtering[13] have already been demonstrated.

II. EXPERIMENT

The deposition experiments were carried out in a single wafer ALD reactor that was developed and build by the IMOS group. It is a low-pressure system equipped with a dry vacuum pump. The reactor is a cold-wall system but is equipped with an inner liner that is heated by the susceptor plate. Liquid precursors can be heated to adjust their vapor pressures that are measured by temperature-corrected pressure gauges. Dosing is achieved by "vapor-draw" by fast acting valves, and transport can be supported by nitrogen carrier flow. The plasma was generated by a capacitively coupled plasma source "epilogos" developed by Sentech Instruments GmbH and Ferdinand-Braun-Institut, Berlin. This source is built up of a 2×2 array of ceramic capillary tubes, wherein the plasma generation takes place, and was mounted as compact module on the top plate of the ALD reactor. No valve is needed between the reaction chamber and the plasma module since already small amount of gas flow through the capillary tubes blocks backflow of unwanted species. For each discharge tube a GaN microwave power oscillator at about 2.45 GHz is powered by a common 28 V dc supply with an input power of about 112 W. The power delivered to the plasma is greater than 10 W for each of the four resonators. Plasma ignition is simply set by switching on the oscillators using a digital signal pulse from the control system. Fast and reproducible ignition is possible for the gas flow of 50 sccm of pure oxygen. The flow density of atomic oxygen was measured by a nickel probe for 200 and 300 sccm gas flow to be $5 \times 10^{15}\,cm^{-2}s^{-1}$ and $8 \times 10^{16}\,cm^{-2}s^{-1}$, respectively. For the experiments, 100 sccm oxygen was fed through the plasma head while the inlet of the vaporized precursors is located below the plasma source above the top plate of the reaction chamber. The ALD system is loaded by a load-lock and dealer transfer system under vacuum conditions. Attached to the same transfer cluster is the rapid thermal processing system (RTP), where the doping experiments could be carried out without exposing the deposited samples to ambient air. It is a modified "Hector" RTP-Cluster-Module from Steag AST (now Mattson Technology, Inc.), which allowed low-pressure single wafer processing by radiation heating with 16 tungsten halogen lamps through a quartz pane from below. The temperature homogeneity across the whole wafer is rather poor with the only one lamp field available. The wafer is placed on three quartz pins, one of which has an integrated thermocouple (TC) for direct temperature measurement. The position of the TC is close to the wafer edge, thus not allowing an accurate control of the temperature in the central part of the wafer. Temperature correction was carried out by evaluating the lamp power during processing of a test wafer with an integrated thermocouple. Due to some delay in temperature response of the TC, the real wafer temperature peaked at the end of the ramp-up phase quite above the target temperature. The maximum temperature at this point was assumed to have highest impact on the overall diffusion process and therefore was taken as reference for the analysis of the doping results. Silicon wafers of 150 mm diameter were used as substrates or silicon samples cut into $15 \times 15\,mm^2$ pieces and placed on carrier wafers. All samples were n-type phosphorus doped in order to obtain pn-junctions at the surface by the boron doping. The boron precursor that was used for the deposition processes was tris(dimethylamido)borane ($B(NMe_2)_3$ or (TDMAB) from Sigma-Aldrich (SAFC). This precursor is relatively inexpensive and has suitable vapor pressure for "vapor-draw" precursor delivery. The vapor pressure depending on the temperature was reported in the literature[14]

$$\log\left[p(\mathrm{TDMAB})/\mathrm{Pa}\right] = -2476/(\mathrm{T/K}) + 1.75\log(\mathrm{T/K}) - 0.0039086(\mathrm{T/K}) + 7.94393. \quad (1)$$

The vapor pressure was stabilized at about 6500 Pa by precursor container heating to 70 °C. Vapor containing lines were generally kept at 120 °C in order to surely avoid any condensation of vapor. The deposition cycles consisted of several substeps that could be individually defined. Typical sequences for the TDMAB precursor (init/pulse/exposure/purge) were 3 s/25 ms/6 s/15 s and for oxygen (init/plasma/exposure/purge) 1 s/10 s/2 s/15 s. The processes were not further optimized in terms of throughput, shorter purge and exposure times might be applicable.

The oxide thickness was measured *ex-situ* by spectroscopic ellipsometry with an SE 850 from Sentech Instruments GmbH by using a wavelength range from 320 to 800 nm. A time delay between deposition and *ex-situ* measurement could not be avoided but is relevant in the case of air-sensitive boron oxide layers. The clean room air humidity was generally kept at about 50%, but individual humidity control or adjustment for the time the samples were exposed to the clean room air could not be established. The use of desiccator after deposition and measurement in a humidity controlled environment would help to reduce the error of *ex-situ* thickness measurement but was not available for the investigations. Therefore, automated repetitions of measurements were programmed for air exposure time dependent thickness monitoring on the same spot. The sheet resistance

measurements were carried out by an ordinary four-point probe (FPP) setup (CDE ResMap168). During the measurements, the samples were exposed to the clean room air, but shielded from direct light incidence. Four collinear tips of 40 μm radius and 1.58 mm apart were pressed onto the surface by a constant spring load of 1.96 N. Measurements through thin oxides with thicknesses up to about 4 nm were possible with these tips. A sheet resistance value was calculated from measured I–V-curve of about 2000 I–V pairs. The maximum current was about 70 μA. The quality test of each measurement for proving ohmic behavior of the resistance and the optimization to minimum currents for sufficient voltage readings was automatically done by evaluating the linearity of the I–V curve quantified by a figure of merit. Measurement reproducibility investigation, carried out by repeated pressing of the tips onto the surface, showed results better than 0.5%. However, such repeatability tests produce mechanical stress or structural damage on the surface and were not performed on each sample. Repeated measurements with continuous tip contact on the surface resulted in reproducibility better than 0.03%. The long term stability of the samples in clean room environment depended on the doping level. A time dependent increase in sheet resistance[7] was observed for all doped samples with higher increase for samples with higher R_S but insignificant increase for sheet resistance below 400 Ω/sq. For example, an increase of about 1.4% in 15 h was observed for a sample with 370 Ω/sq. In general, the sheet resistance measurements were carried out 3 h after the doping process. A Cameca IMS Wf SIMS system was used for boron profiling. An oxygen beam of 1 keV energy was applied for boron analysis. A silicon standard sample implanted with known boron dose was used for calibration. Initially, the standard sample was measured, and the relative sensitivity factors were calculated. These factors were then used for quantification. The chemical analysis was carried out by XPS in an ESCA 5600 of Perkin Elmer. Mg Kα radiation was used as x-ray source. Argon sputtering for depth profiling was applied on $3 \times 3\,mm^2$ wide areas with 4 kV accelerated Ar ions. Furthermore, scanning electron microscope (SEM) images could be obtained by this system using electron beam of 2 kV and 10 nA at 45° impact angle.

III. RESULTS AND DISCUSSION

A. Growth investigation

ALD type growth could be achieved using the TDMAB precursor with oxygen radicals generated by the remote plasma source. No growth was obtained using oxygen or TDMAB alone.[8] Experiments were carried out in order to prove saturation coverage for each precursor exposure. At room temperature, (20 °C) 25 ms pulse time was sufficient to reach saturation (Fig. 2) for TDMAB pulse as shown in Fig. 1, while about 15 s oxygen plasma exposure time was needed for full saturation. However, most experiments were carried out with 10 s plasma exposure time as the film thickness homogeneity and reproducibility was already sufficient and the total process time and plasma load could be decreased.

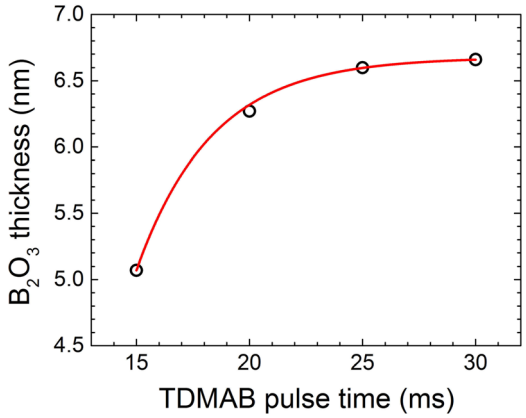

FIG. 1. (Color online) Boron oxide thickness depending on the pulse time of the TDMAB precursor, 50 cycles of deposition at 20 °C, and 10 s oxygen plasma.

The boron oxide film thickness decreases in air until stable final coverage is reached, see Fig. 3. This behavior was reported before.[7] For the present PALD experiments, this final coverage is higher for thicker initial layers and the rate of decrease seems to be generally higher for the thicker films. For these films, more rapid decrease was observed during the first couple of minutes when exposing to air. These might be effects of the total longer plasma exposure during growth of the thicker films. The stability of the as-deposited film thickness was evaluated by extrapolating the slope of the initial decrease to the time zero that was defined by taking out the samples from the vacuum load lock. These slopes are shown in Fig. 3 as black lines. The effect of different ambient conditions, especially humidity levels, could be considered individually for each sample by this procedure.

The reason for this type of almost complete volatilization, which was also observed by Kim *et al.*,[10] is not quite clear. Sokolov[15] reported substantial relaxation of CVD-produced borophosphosilica glass films (BPSG) during their storage in air. Interestingly, it was found that the boron-loss is significantly higher from BPSG compared to those that did not contain phosphorus (BSG). Furthermore, storage in air led to increase of thickness and oxygen content. Sokolov discussed a mechanism of dielectric degradation wherein boron oxide

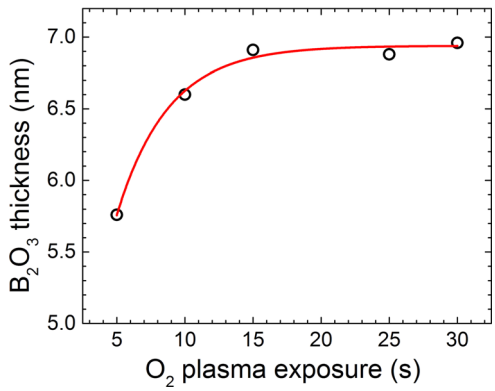

FIG. 2. (Color online) Boron oxide thickness depending on the oxygen plasma exposure time, 50 cycles of deposition at 20 °C, and 25 ms TDMAB pulse.

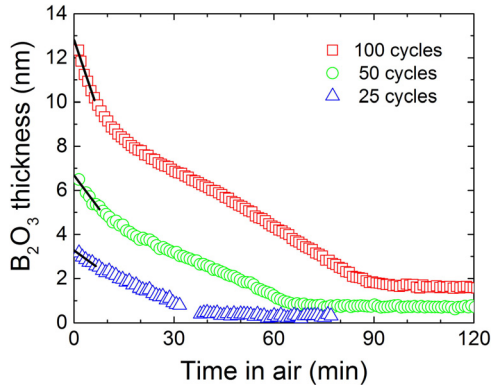

FIG. 3. (Color online) Results of time-dependent measurements of film thickness in air: PALD of B_2O_3 at 20 °C with different number of cycles. The initial slopes of decrease are shown as black lines.

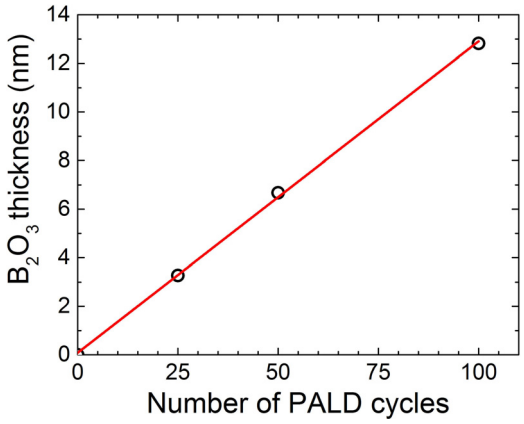

FIG. 4. (Color online) Thickness of the as-deposited boron oxide vs number of PALD cycles at deposition temperature of 20 °C.

charging is involved, leading to boron movement to the surface when both dopants, boron and phosphorus, are present in the films. This should explain the observed significant boron out-gassing even at room temperature. However, the very mechanism for the boron escape from the material is not explained by this mechanism. It is only suggested that the probability for boron to leave the BPSG upon reacting with H or to form other volatile complexes is increased when the charged $[BO^4]^-$ complexes have arrived at the surface. From investigation of wear properties of B_2O_3[11] it was concluded that spontaneous transformation of its surface in air results in boric acid (H_3BO_3), which is responsible for its application as solid lubricant. But no kind of volatilization was reported from their boron oxide samples. Only changes of color were observed. Freshly fractured surfaces were transparent but rapidly became cloudy in ambient air. A similar effect was observed by Putkonen and Niinistö[8] on their uncapped ALD boron oxide films. Detailed investigation of the vaporization of boric acid was carried out by Balasubramanian *et al.*[16] X-ray diffraction measurements and Knudsen effusion mass spectrometry showed that H_3BO_3 vaporizes without decomposition and H_3BO_3 (g) was the principle vapor species in the whole investigated temperature range of 295–342 K. Their calculated and recommended Antoine equation for the equilibrium vapor pressure of solid boric acid in the temperature range from 295 to 413 K is given as

$$\log\,[p(H_3BO_3)/Pa] = -(5199\pm74)/(T/K) + (15.65\pm0.23). \quad (2)$$

Hence, the vapor pressure of H_3BO_3 at a temperature of 22 °C can be expected to be 1.08×10^{-2} Pa and seems to be quite low to explain the fast volatilization. Maybe, in our case, the preceding exothermic reaction of the boron oxide with water could additionally promote its volatilization as boric acid in humid air.

The dependence of the as-deposited layer thickness on the number of PALD cycles is shown in Fig. 4. As in the case of thermal ALD with ozone,[7] no delay in the initial phase of the growth of the films was observed for the PALD and the film thickness increases linearly with the number of cycles, which is favorable for boron source control for the doping application where only very thin layers of boron oxide are needed. Growth per cycle (gpc) was calculated from measurements of samples that received 50 deposition cycles each. The error for the individual thickness determination, which means after calculations from the spectroscopic measurement of the ellipsometric angles, was estimated from repeated measurements and simulated thickness variations to be less than 0.1 nm. The same model[7] was used for all the measurements. The model was not calibrated by independent thickness measurements as, for example, by TEM analysis, because of the instability of the boron films. Therefore, the absolute values of the boron oxide thickness might contain some error, but comparisons of results of different deposition processes are reliable. At room temperature, the gpc was approximately 0.13 nm, and it decreases as the deposition temperature is increased, as it can be seen in the trend in Fig. 5. The possible reason for this behavior could be precursor desorption at higher temperature thereby reducing the surface reaction sites, or increased volatilization of the already grown film after reaction with traces of moisture in the deposition chamber at higher temperature. The gpc was higher for the reaction with the atomic oxygen

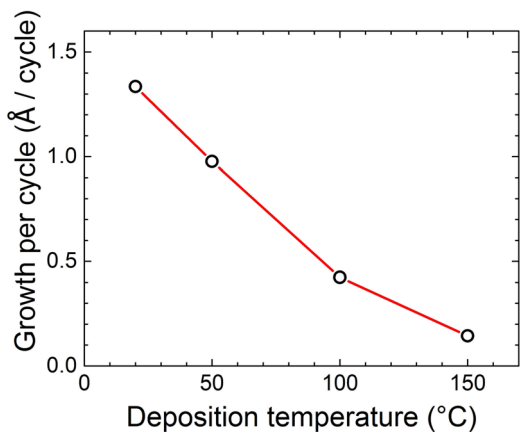

FIG. 5. (Color online) Growth per cycle during PALD of boron oxide depending on the deposition temperature.

radicals from the plasma process compared to thermal atomic layer deposition of boron oxide using the same boron precursor with ozone as oxidant.[7]

Since boron oxide is moisture sensitive, some samples of boron oxide were prepared and capped with antimony oxide for further analysis of the film as it was reported before.[7] Capping is indispensable if samples need to be handled in air. Boron oxide film of about 26 nm (200 cycles) was deposited on silicon substrate at room temperature, and this sample was capped with about 11.5 nm (150 cycles) of antimony oxide grown at 200 °C. The individual layer thicknesses were measured on separate samples. The capping deposition was carried out after heating the susceptor to the higher temperature, needed for the antimony oxide deposition using trimethyl antimony and oxygen plasma. The capping layers itself proved to be very stable in air. The layer stack of the capped sample was measured by ellipsometry and fitting a two-layer model resulted in thicknesses of only 14.6 nm of boron oxide below 6.1 nm of antimony oxide, which is less compared to the results from the single layers' depositions. Some boron oxide might have been lost at the capping deposition temperature of 200 °C, before the capping was effective. Moreover, the initial growth rate of antimony oxide on the boron oxide could be retarded compared to that on the silicon substrate, which was used for reference. Several repeated measurements on this layer stack after storage in air showed no sign of layer diminution, instead a slight increase of the total thickness could be observed. After more than 16 weeks of storage in air the measured thickness increased to 19.6 and 6.3 nm of boron oxide and antimony oxide, respectively. Diffusion of moisture through the capping could explain this observation. Minimal swelling of the boron oxide film would result from its degradation due moisture uptake or chemical reactions. Similar observations of Sokolov on doped glass films[15] seem to support this conclusion.

The antimony oxide capped sample was then analyzed in the vacuum of the XPS system equipped with scanning electron microscope. Interesting features of film deformation could be found, which are shown in Figs. 6 and 7. White spots of similar diameter surrounded by circular halolike areas can be observed on the nonsputtered sample. In the very center of each of white spots little dark dots are visible. Besides this, some scratches with distinct angles to each other can be seen in Fig. 6, the smaller ones consisting of traces of individual dots. After sputtering, the gray levels of the image were practically inverted, as shown in Fig. 7. The formerly white areas appear darkest now and the traces of small dark dots are clearly visible. The edge of the sputtered area can be seen in the upper part of this image where white spots are still visible.

Additionally, other areas of the film stack, not having been affected by the electron beam of Ar ions before and seemed to be intact at the beginning of the SEM investigation, were gradually degrading in the process of image formation. Progressive bulging of film on the electron beam affected area could be observed during image renewal. A possible explanation for the observed features of degradation could be that some boron already reacted to boric acid below the capping, which produced high stress in the films. Already by putting it into vacuum, some areas of the film could have been ripped due to the pressure change. Additionally, the energy dissipation into the films from the electron beam might have promoted the degradation reactions. Buc *et al.*[13] reported about a similar phenomenon during selected area electron diffraction measurements on magnetron sputtered boron oxide films. Their images showed instabilities due to vaporization of H_3BO_3 crystallites upon electron beam exposures. They concluded that after exposure of boron oxide films to ambient air H_3BO_3 crystallites form which vanish due to electron beam heating and eventual dehydration. They also found that these crystallites

FIG. 6. (Color online) Scanning electron microscope image of a boron oxide sample capped with antimony oxide after storage of more than 16 weeks in air. The picture was taken before argon sputtering.

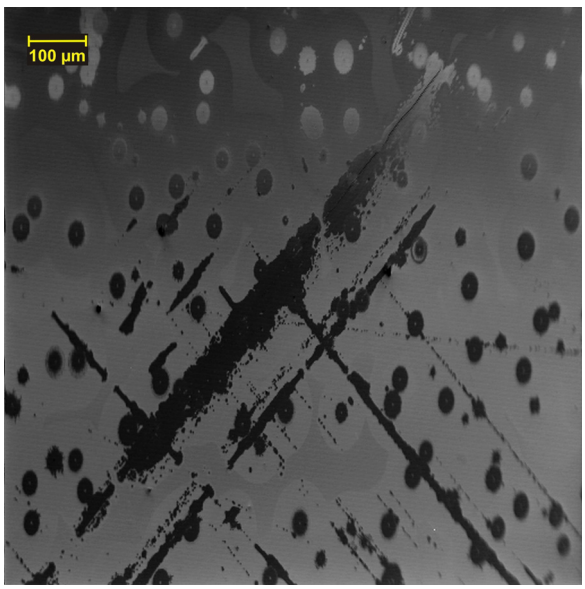

FIG. 7. (Color online) Scanning electron microscope image of the sample of Fig. 6 after one minute of argon sputtering.

transformed to cubic HBO_2 phase before completely vanishing. On our sample, boron without carbon contamination could still be detected below the antimony oxide capping by XPS analysis after 1 min of sputtering on a spot size of about 0.8 mm diameter within the sputtered area. Some of the capping seemed to have been still intact. Time-dependent degradation could also be observed in real-time by optical microscopy. The stability of different film stacks did not only depend on the thickness of the capping layer, but also on the thickness of the B_2O_3 film. Thicker B_2O_3 films led to faster degradation of the samples. Thicker B_2O_3 is believed to produce stress in the capping film, which could result in some sort of crack formation. Starting from those imperfections and from the edges of the samples, bubblelike features, which could be easily observed by an optical microscope, appeared and grew on a time scale of hours or days. More detailed investigation on these phenomena needs to be conducted. However, an application of the peculiar moisture sensitivity of boron oxide films for probing capping properties of moisture barriers or passivation layers seems to be feasible, especially for ALD grown films, since the moisture detector (B_2O_3) and the barrier layer to be evaluated could be grown *in-situ*. Thereafter, the change of the boron oxide film properties, which results from its sensitivity to moisture, can be easily monitored in different environments. This can be carried out, for example, by direct observations with optical microscopes or simple automated time and position dependent measurements of the film's thicknesses or optical constants with sufficient precision. Existing methods for analysis of moisture barrier properties of capping materials, which is especially important for the growing application of flexible and organic electronics, are mostly carried out by using calcium.[17] This material cannot be deposited by ALD and its application is therefore rather complicated.

B. Rapid thermal anneal experiments

Samples of uncapped boron oxide were prepared on n-type silicon at room temperature by the PALD process and directly transferred into the rapid thermal process chamber for RTA in 5 mbar oxygen without breaking the vacuum. At first, three different samples with the same number of 25 deposition cycles were annealed at different temperatures. Equal ramp rates of about 11.5 K/s and soak times of 5 s were applied. After the annealing process, the sheet resistance of the samples was measured by four-point probe method through the remaining oxide layer, the oxide thickness was measured by ellipsometry, and the boron concentration in the sample was measured by SIMS. All the SIMS profiles showed a distinct peak of the boron concentration at the sample surface. It is quite difficult if not impossible to unambiguously elucidate the nature of the boron occurrence there.[18] The peak height is partly a SIMS measurement artifact due to nonequilibrium in sputter rate and secondary ionization, the peak slopes are to some extent governed by ion mixing effects, and depth scale is affected in this region because of sputter-rate deviation with respect to the sputter rate of the silicon matrix, which is assumed constant and used for calibrating the overall depth scale. Hence, it is not clear from the SIMS profiles alone whether and how much of the boron remained in the source layer or in an oxidized part of the silicon interface region and how much is incorporated and furthermore active in the silicon matrix there. However, the measured boron concentration apart from that peak region deeper in the silicon and above the measurement limit of the SIMS is regarded as quantitatively correct. Therefore, further analysis was carried out referring to the results from the electrical measurements of the sheet resistances. An example of the boron concentration profiling of one sample is given in Fig. 8. Here, the original SIMS profile is shown in green color in the background. This profile was fitted in two regions with two separate Gaussian curves in order to construct a theoretical boron profile. One fit was used to extrapolate the reliable section of measured profile to the surface and the other one fitted the region deeper into the bulk below the measurement limit of the SIMS. The Gaussian fits approximated very well in the particular regions as can be seen in Fig. 8 by comparing the original SIMS profile with the fitted curve composed of the two Gaussian curves. (The deviation of the fit from the measured profile at its deeper edge just above the SIMS measurement limit could be caused by evolving crater bottom roughness from the sputtering process and ion-mixing effects. Nevertheless, this deviation has insignificant impact on the sheet resistance calculations.) The reason of the occurrence of the altogether "stretched" Gaussian diffusion profile was not further analyzed here with respect to the annealing conditions, such as temperature profile, annealing ambient, etc., since the exact temperature profile during the annealing process was not sufficiently well known. However, the Gaussian curve shape points toward limited source situation prevailing and the distortion to more boxlike form indicates diffusion enhancement due to high-concentration effects or surface oxidation. Further investigation including process simulation tools needs to be carried out for better understanding.

Here, the profiles were analyzed by calculating the sheet resistance using physical based mobility models within the device simulation software ATLAS from SILVACO, Inc. Klaassen's unified low field mobility model[19,20] was used

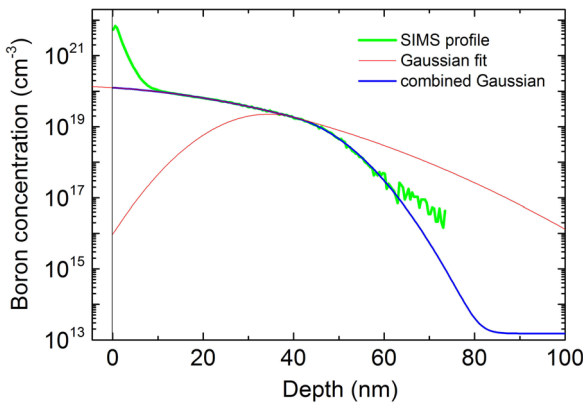

FIG. 8. (Color online) Measured SIMS profile of boron concentration in silicon after RTA (profile with surface peak) and supposed boron concentration profile in the bulk silicon (thick line) composed of two Gaussian fits (thin lines).

for the description of the carrier mobilities including temperature dependent effects of lattice scattering, impurity scattering, carrier–carrier scattering, and impurity clustering effects at high concentrations.[21] The sheet resistance was calculated by

$$R_S = \left(q \int_{x_0}^{x_j} [\mu_n(x) \cdot n(x) + \mu_p(x) \cdot p(x)] dx \right)^{-1},$$

where q is the elementary charge, x is the depth of the profile, x_0 its starting point, x_j is the junction depth, μ_n and μ_p are the electron and hole mobilities, and n and p are the electron and hole concentrations, respectively. The carrier mobilities and concentrations were calculated from the modeled dopant profiles, whereas contribution of the electron minority carriers could be neglected for the present situation. An example of the comparison of sheet resistance calculations with the result of the measured value of the sample of Fig. 8 is given in Fig. 9.

The calculation of the sheet resistance from the measured SIMS profile, assuming the boron concentration in the peak above the Gaussian distribution of certainly electrically active boron in the silicon, is *not* contributing to the silicon doping results in too high value of sheet resistance. Therefore, it can be concluded that

(1) The boron concentration peak is not only an SIMS measurement artifact.
(2) This boron is not only located in a remaining source layer or inside oxidized silicon but also incorporated into the silicon matrix.
(3) A significant share of this boron is active in the silicon.

Further calculations were carried out taking into account different amount of the measured boron concentration by simply cutting off increasing portion of the topmost parts of the boron concentration profile but including the peak concentration until the calculated value of the sheet resistance from the remaining profile matched the measured one. The result of this analysis is shown in Fig. 9 as well. This

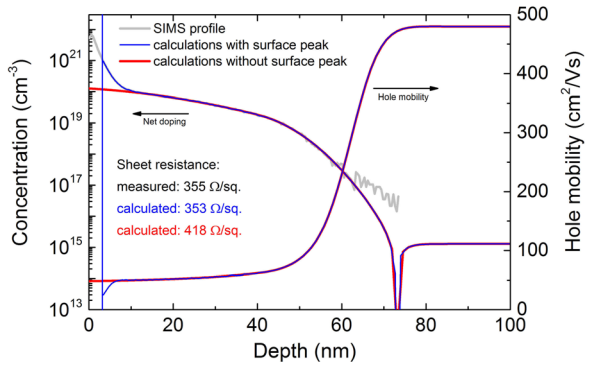

FIG. 9. (Color online) Example of comparison of sheet resistance calculations with measured sheet resistance. Calculated sheet resistance from whole profile but neglecting surface peak results in to high value, calculation including part of the peak boron concentration as indicated matches measured value. (Calculated hole mobility values are shown on the right axis.)

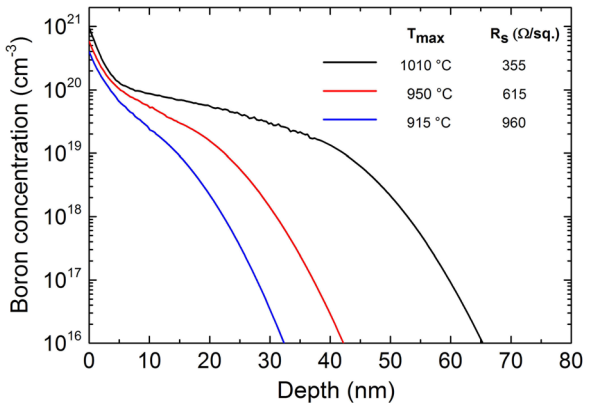

FIG. 10. (Color online) SIMS measured boron concentration profiles in silicon of three different samples with equal initial B_2O_3 thickness of about 3.3 nm after different RTA treatments. The profiles were cut and aligned to match the calculated sheet resistance values from the profiles with the measured ones.

procedure gives an idea where the interface between the Si and the oxide could be and how much of the boron concentration of the peak region might be active. However, it should be pointed out here that these results are not necessarily quantitatively certain since the hole mobility, which is included in the calculations, depends significantly on the (real) concentration in the high concentration region and the (real) shape of the peak of the boron concentration in silicon will differ from the one that was obtained here from the SIMS measurement as discussed before. More thoroughly peak analysis in the surface and interface region needs to be carried out to elucidate this in detail. Nevertheless, this method was applied to all the measured profiles in order to compare the effect of the different treatments with respect of the doping effect in the silicon and to comparably exclude inactive boron from the surface region.

In Fig. 10, the SIMS profiles of the three samples with equal initial B_2O_3 thickness that were differently heat treated are shown for comparison. The profiles were cut and aligned according to the procedure explained above; zero depth would be here at the position at which the silicon matrix begins. One can see that the profiles have similar shape, and they show no sign of depletion of the B_2O_3 dopant source of about 3.3 nm initial thickness since the peak concentration of

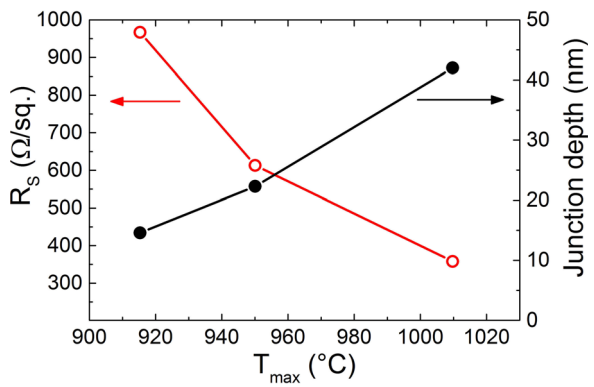

FIG. 11. (Color online) Dependence of the sheet resistance and the junction depth on the maximum annealing temperature of the samples of Fig. 10.

TABLE I. Results of temperature variation experiments. All samples had initially 3.3 nm B_2O_3 thickness (25 ALD cycles), RTA in 5 mbar O_2, ramp rates of about 11.5 K/s, and soak times of 5 s.

T_{max} (°C)	Oxide thickness (nm)	Profile shift (nm)	R_S (meas.) (Ω/sq.)	R_S (calc.) (Ω/sq.)	$z_{j(19)}$ (nm)	z_j (nm)	C_{Bmax} (cm^{-3})	Dose (cm^{-2})
915	4.59	4.96	967	994	14.6	35.9	3.95×10^{20}	1.16×10^{14}
950	5.16	5.37	613	625	22.3	46.1	5.80×10^{20}	1.96×10^{14}
1010	4.64	3.35	358	353	40.0	69.2	9.70×10^{20}	3.68×10^{14}

boron did not saturate or drop with higher temperature. Instead, higher temperature during RTA resulted in deeper diffusion of more boron into the silicon and lower sheet resistances whose measured values are listed in Fig. 10.

The dependence of the sheet resistance and the junction depth (which is defined here at the point where the boron concentration falls below $1 \times 10^{19}\,cm^{-3}$, a typical situation in ultra-shallow doping regions of MOS devices) on the maximum annealing temperature is shown in Fig. 11.

The results of the analysis of the experiments on temperature variation of the RTA process are summarized in Table I. Here, T_{max} is the maximum temperature of the RTA process, the oxide thickness is the thickness of the surface layer after the RTA process, the profile shift is the depth that was cut from the top of the measured SIMS profiles in order to obtain the given calculated sheet resistance value [R_S (calc.)], while R_S (meas.) is the sheet resistance measured by four point probe after the RTA. The junction depth $z_j(19)$ is the profile depth at a boron concentration of $1 \times 10^{19}\,cm^{-3}$, z_j is the junction depth, C_{Bmax} is the maximum boron concentration in the silicon matrix (at the interface), and the dose is the sheet concentration of boron in the silicon.

In a following set of experiments, samples with different amount of B_2O_3 source were annealed. They received different number of deposition cycles but similar RTA treatments. Here, faster ramp rates of about 16.7 K/s and no soak time were applied. The results of SIMS measurements after the RTA are shown in Fig. 12. Due to reproducibility issues of the RTA processes, slightly different peak temperatures were effective as listed in the figure, but qualitative comparison can still be carried out.

For less than 15 cycles of B_2O_3 deposition, the boron source at the surface depleted at the present RTA conditions. The maximum boron concentration and a plateaulike section of the profiles shift to lower boron concentrations for less initial B_2O_3 coverage as boron diffuses into silicon. On the other hand, the diffusion of boron into silicon seems to be slower for thicker surface coverage of boron oxide compared to the 15 cycle sample. Increasingly higher sheet resistance was measured and profiles with shallower junction depth were obtained. The results of sheet resistance measurements and profile analysis are given in Fig. 13. The junction depth (at $C_B = 1 \times 10^{19}\,cm^{-3}$) was obtained from the profiles relative to the depth of the maximum of the peak at the assumed begin of the silicon matrix, i.e., after the alignment as shown in Fig. 12. The initial thickness of the boron oxide source layer seems to affect the diffusivity of the boron in the silicon. This behavior might be related to the presence of oxygen in the annealing atmosphere. Oxygen could easily reach the silicon interface though the very thin layers and cause silicon oxidation, which can promote oxidation enhanced diffusion of boron. The thicker initial boron oxide layers might reduce this effect by retaining oxygen and suppressing silicon surface oxidation. Another reason could be stress in the silicon interface induced by the thicker boron oxide films, which retards the diffusion compared to the thinner boron oxide films.

The dose of (active) boron in the silicon after RTA, calculated from the integration of the SIMS profiles, is also shown in Fig. 13. More boron was found in silicon after RTA with increasing initial B_2O_3 thickness up to 2 nm (i.e., after 15

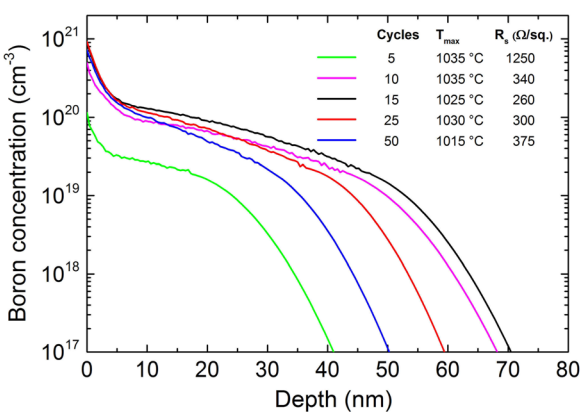

FIG. 12. (Color online) SIMS measured boron concentration profiles in silicon of samples of different thickness of initial B_2O_3 source treated with similar RTA processes. The profiles were cut and aligned to match the calculated sheet resistance values from the profiles with the measured ones.

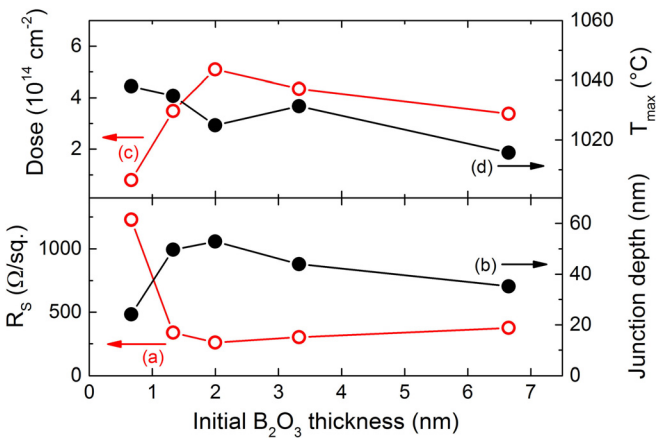

FIG. 13. (Color online) Dependence of the sheet resistance (a), junction depth (b), and measured total boron dose (c) on the initial ALD B_2O_3 thickness of the samples of Fig. 12. The peak temperatures of the RTA processes (d) are shown for reference.

TABLE II. Results of experiments of source thickness variation. RTA in 5 mbar O_2, ramp rates of about 16.7 K/s, and no soak.

ALD cycles	B_2O_3 thickness (nm)	T_{max} (°C)	Oxide thickness (nm)	Profile shift (nm)	R_S (meas.) (Ω/sq.)	R_S (calc.) (Ω/sq.)	$z_{j(19)}$ (nm)	z_j (nm)	C_{Bmax} (cm^{-3})	Dose (cm^{-2})
5	0.7	1038	2.3	0.58	1230	1126	24.1	50.3	2.44×10^{20}	0.79×10^{14}
10	1.3	1035	3.2	1.47	339	343	49.7	78.5	4.90×10^{20}	3.49×10^{14}
15	2.0	1025	4.4	3.24	260	255	52.9	80.0	8.78×10^{20}	5.10×10^{14}
25	3.3	1031	4.9	5.01	302	303	44.0	68.0	9.19×10^{20}	4.35×10^{14}
50	6.6	1016	6.4	7.67	376	382	35.2	58.9	7.16×10^{20}	3.38×10^{14}

ALD cycles). The dose did not further increase for initially thicker deposited samples but rather decreased, and more boron remained in the source layer at the surface. The latter is, however, not shown Fig. 12, as this section was cut off from the SIMS profiles for alignment. This can be related to slower diffusion for these samples. The different peak RTA temperatures are also shown in Fig. 13 for comparison but their variations seem not to be the reason for the discussed dependences of the process results.

The results of the analysis of the annealing experiments with samples of different initial thickness of boron oxide deposited by PALD are given in Table II.

Furthermore, the influence of repeated annealings on the boron diffusion from the atomic layer deposited surface source layer was investigated. Samples with different thickness of B_2O_3 were treated with the same RTA process conditions as applied before (ramp rates of about 16.7 K/s and no soak time). Three samples were annealed at once, and the sheet resistances were *ex-situ* measured after the RTA. The film of remaining B_2O_3 and grown SiO_2 was not removed from the surface after the RTA. This procedure was repeated four times so that these samples received in total five nearly identical RTA treatments. They were analyzed by SIMS and the results were compared with those obtained from samples that were heat treated only once (with the same RTA conditions). The SIMS profiles of these samples aligned according to the procedure discussed above is shown in Fig. 14.

The comparison of the SIMS profiles shows that most of the boron diffusion happened already during the first RTA process. The increase in junction depth during this process was higher than that resulting from the four following annealings altogether. One can also see from the profile's comparison that the faster diffusion from the thinnest source layer, leading to the greatest junction depth after the first RTA, seemed to persist during the following heat treatments. While for the thicker source layers the junction depth (and so the sheet resistance) tended to equal the difference to the junction depth from the thinnest source layer rather increased. This behavior becomes also evident in the change of the sheet resistance after each sequent RTA as shown in Fig. 15.

The magnitude of the decline of the sheet resistance is decreasing with each RTA run, and for the lowest initial source layer thickness, it reached almost a saturated value already after the second run. This is an indication of the beginning of the depletion of this source, which can also be seen on the profile in Fig. 14 where the height of the plateau of the boron concentration of this sample with 15 ALD cycles after five times RTA is lower than those of the other two. It seems that the initially incorporated boron dose cannot be raised anymore by this type of rather slow annealings. This is also illustrated in Fig. 16. The calculated sheet concentration of boron in silicon is almost constant for the sample with 15 initial ALD cycles, rather little loss of boron is detected. The reason for this can be outdiffusion or trapping into the growing SiO_2 layer. For the initially thicker

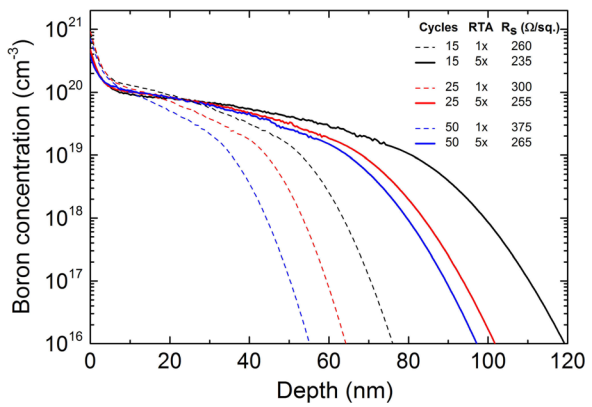

FIG. 14. (Color online) SIMS measured boron concentration profiles in silicon of samples of different amount of initial B_2O_3 source after one time RTA in comparison with profiles of samples that received five sequent annealings. The profiles were cut and aligned to match the calculated sheet resistance values from the profiles with the measured ones.

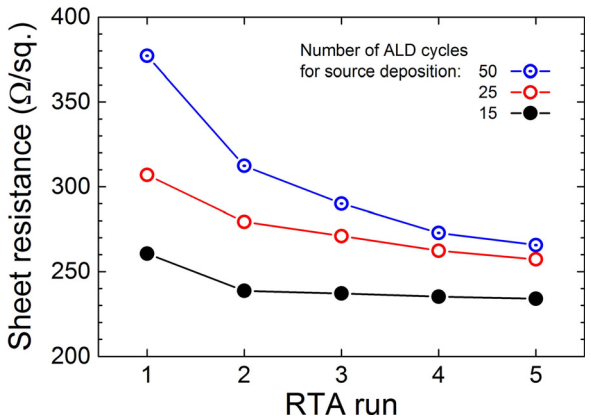

FIG. 15. (Color online) Dependence of the sheet resistance on the number of sequent RTA processes for three samples of different initial boron oxide thickness.

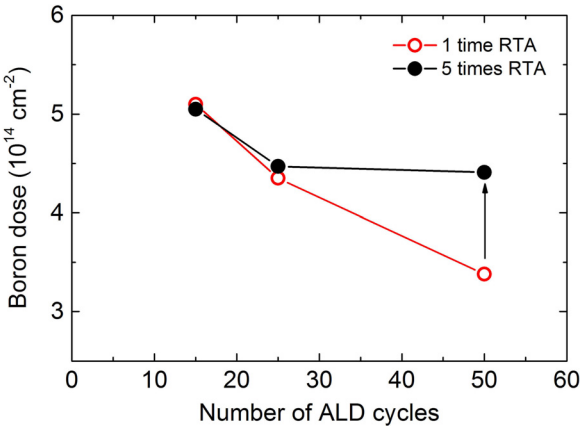

FIG. 16. (Color online) Comparison of the (active) boron dose in the silicon after one time RTA and five times RTA for three samples of different initial boron oxide thickness.

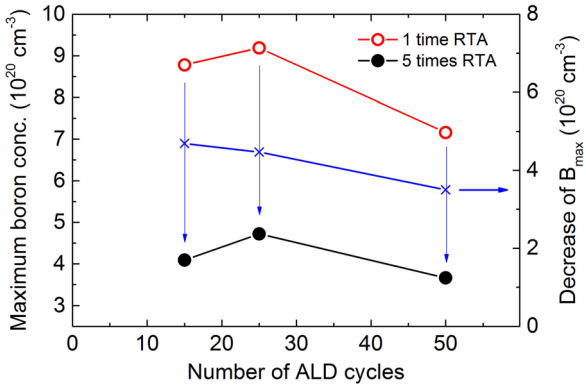

FIG. 17. (Color online) Comparison of the maximum boron concentration in the silicon matrix at the interface after one time RTA and five times RTA for three samples of different initial boron oxide thickness.

films, more boron is incorporated by the multiple annealings. However, the amount of boron that was introduced from the thinner source layer was not reached by the thicker films' annealings, which is also evident from the sheet resistance results. The doping seems to be most effective for an optimum *thin* layer, if the layer is too thin the source depletes too rapidly, if is too thick the diffusion is retarded and so the amount of boron incorporation. The optimum thickness will however be depending on the chosen RTA conditions.

The extracted maximum boron concentration is presented in Fig. 17. With cut-off from the top of the profiles for alignment part of the peaked boron at the surface was supposed to be active in silicon as discussed before. Its maximum at the beginning of the aligned profiles is an indication of the position of the Si/SiO_2 interface where maximum of active boron above the Gaussian part of the profiles exist. The absolute value of this might contain some error but qualitative comparison can be carried out here nevertheless as given in Fig. 17.

The maximum concentration decreased for all samples after five RTA treatments compared to the first one, which is an indication of the decrease of the effectiveness of the remaining dopant source with sequent heat treatments. Furthermore, the magnitude of the decrease is highest for the sample with the thinnest B_2O_3 source layer supporting the evidence for the faster depletion of this dopant source. Finally, the extracted results from the experiments with sequent annealings are summarized in Table III.

IV. SUMMARY AND CONCLUSIONS

Boron oxide films have been deposited by plasma-assisted atomic layer deposition on silicon substrates using TDMAB and oxygen radicals. Linear ALD type growth behavior was obtained without incubation cycles, and growth saturation was proven for TDMAB exposure as well as for oxygen plasma exposure. Highest growth per cycle of 0.13 nm was achieved at room temperature. Boron oxide film can also be grown at higher temperature up to 150 °C but with almost linear with temperature decreasing growth per cycle. An instability of the boron oxide in ambient air is caused by reaction of the film with moisture to result in boric acid. This reaction can be retarded by a capping layer of *in-situ* grown antimony oxide. The application of the boron oxide for monitoring moisture barrier properties of capping films, particularly for those grown by ALD, is suggested. Easy to grow ALD B_2O_3 can be capped *in-situ* by the material to be investigated, and the film stack can be analyzed by optical microscope or ellipsometric measurements in a testing environment. Shallow boron doping of silicon could be obtained by using the boron oxide layers as dopant source. The thickness of the source layer needs to be optimized with respect to the RTA conditions. For very thin layers of <2 nm, the source tends to deplete too quickly and might therefore not be sufficient depending on the doping requirements. Proper thickness control, which can be achieved by ALD processes, is important since the thickness of the dopant source layer at the surface has impact on the diffusion process inside the silicon. The ALD method allows

TABLE III. Results of repeated annealings. RTA in 5 mbar O_2, ramp rates of about 16.7 K/s, and no soak.

ALD cycles	B_2O_3 thickness (nm)	No. of RTA	Oxide thickness (nm)	Profile shift (nm)	R_S (meas.) (Ω/sq.)	R_S (calc.) (Ω/sq.)	$z_{j(19)}$ (nm)	z_j (nm)	C_{Bmax} (cm^{-3})	Dose (cm^{-2})
15	2.0	1	4.4	3.24	260	255	52.9	80.0	8.78×10^{20}	5.10×10^{14}
		5	5.3	5.26	238	236	80.5	126.0	4.09×10^{20}	5.05×10^{14}
25	3.3	1	4.9	5.01	302	303	44.0	68.0	9.19×10^{20}	4.35×10^{14}
		5	5.27	6.4	263	266	68.0	107.9	4.72×10^{20}	4.47×10^{14}
50	6.6	1	6.4	7.67	376	382	35.2	58.9	7.16×10^{20}	3.38×10^{14}
		5	6.71	9.58	273	272	64.5	103.2	3.66×10^{20}	4.41×10^{14}

depositing the precise amount of dopant source that is needed for optimum dopant diffusion into the semiconductor depending on the annealing conditions and the formation of excessive dopant glass films during RTA can be avoided. Controlled doping of 3D nanostructured devices by predeposition with ALD source layers should therefore be feasible.

ACKNOWLEDGMENTS

Financial support of the Investment Bank Berlin and EFRE within the framework of the Epilogos project is gratefully acknowledged.

[1]K. Tsutsui *et al.*, J. Appl. Phys. **104**, 093709 (2008).
[2]J. C. Ho, R. Yerushalmi, Z. A. Jacobson, Z. Fan, R. L. Alley, and A. Javey, Nat. Mater. **7**, 62 (2008).
[3]J. C. Ho, R. Yerushalmi, G. Smith, P. Majhi, J. Bennett, J. Halim, V. N. Faifer, and A. Javey, Nano Lett. **9**, 725 (2009).
[4]S. Ingole, P. Aella, P. Manandhar, S. B. Chikkannanavar, E. A. Akhadov, D. J. Smith, and S. T. Picraux, J. Appl. Phys. **103**, 104302 (2008).
[5]G. S. Doerk, G. Lestari, F. Liu, and C. Carraro, Nanoscale **2**, 1165 (2010).
[6]B. Kalkofen, S. Matichyn, and E. Burte, ECS Trans. **19**, 105 (2009).
[7]B. Kalkofen, V. M. Mothukuru, M. Lisker, and E. P. Burte, ECS Trans. **45**, 55 (2012).
[8]M. Putkonen and L. Niinistö, Thin Solid Films **514**, 145 (2006).
[9]B. Kalkofen, A. A. Amusan, M. Lisker, and E. P. Burte, Phys. Status Solidi C **11**, 41 (2014).
[10]W.-H. Kim *et al.*, J. Mater. Chem. C **2**, 5805 (2014).
[11]X. Ma, W. N. Unertl, and A. Erdemir, J. Mater. Res. **14**, 3455 (1999).
[12]O. Moon, B.-C. Kang, S.-B. Lee, and J.-H. Boo, Thin Solid Films **464–465**, 164 (2004).
[13]D. Buc, I. Bello, M. Caplovicova, M. Mikula, J. Kovac, I. Hotovy, Y. M. Chong, and G. G. Siu, Thin Solid Films **515**, 8723 (2007).
[14]E. Wiberg, K. Schuster, and Z. Anorg. Allg. Chem. (Z. Anorg. Allg. Chem.) **213**, 77 (1933).
[15]Y. V. Sokolov, Chem. Vap. Deposition **17**, 22 (2011).
[16]R. Balasubramanian, T. S. Lakshmi Narasimhan, R. Viswanathan, and S. Nalini, J. Phys. Chem. B **112**, 13873 (2008).
[17]J. A. Bertrand and S. M. George, J. Vac. Sci. Technol. A **31**, 01A122 (2013).
[18]W. Vandervorst, T. Janssens, R. Loo, M. Caymax, I. Peytier, R. Lindsay, J. Frühauf, A. Bergmaier, and G. Dollinger, Appl. Surf. Sci. **203–204**, 371 (2003).
[19]D. Klaassen, Solid-State Electron. **35**, 953 (1992).
[20]D. Klaassen, Solid-State Electron. **35**, 961 (1992).
[21]Silvaco, Inc., ATLAS user's manual, device simulation software, Ver. 5.14.0.R.